Biosensors and Bioelectronics xxx (2009) xxx–xxx

Contents lists available at ScienceDirect

Biosensors and Bioelectronics

journal homepage: www.elsevier.com/locate/bios

Quantification of DNA and protein adsorption by optical phase shift

Emre Özkumur[a], Ayça Yalçın[a], Marina Cretich[b], Carlos A. Lopez[a], David A. Bergstein[c], Bennett B. Goldberg[d,a,e], Marcella Chiari[b], M. Selim Ünlü[a,e,d,*]

[a] Department of Electrical & Computer Engineering, Boston University, 8 St. Mary's Street, Boston, MA 02215, USA
[b] Istituto di Chimica del Riconoscimento Molecolare (ICRM), C.N.R., Via Mario Bianco 9, 20131 Milano, Italy
[c] Zoiray Technologies Inc., Boston University Photonics Center, 8 St. Mary's Street, Boston, MA 02215, USA
[d] Department of Physics, Boston University, Boston, MA 02215, USA
[e] Department of Biomedical Engineering, Boston University, 44 Cummington Street, Boston, MA 02215, USA

ARTICLE INFO

Article history:
Received 25 April 2009
Received in revised form 19 June 2009
Accepted 22 June 2009

Keywords:
Label-free detection
Interferometry
Optical biosensor
Microarray
Mass quantification
Biolayer density

ABSTRACT

A primary advantage of label-free detection methods over fluorescent measurements is its quantitative detection capability, since an absolute measure of adsorbed material facilitates kinetic characterization of biomolecular interactions. Interferometric techniques relate the optical phase to biomolecular layer density on the surface, but the conversion factor has not previously been accurately determined. We present a calibration method for phase shift measurements and apply it to surface-bound bovine serum albumin, immunoglobulin G, and single-stranded DNA.

Biomolecules with known concentrations dissolved in salt-free water were spotted with precise volumes on the array surface and upon evaporation of the water, left a readily calculated mass. Using our label-free technique, the calculated mass of the biolayer was compared with the measured thickness, and we observed a linear dependence over 4 orders of magnitude. We determined that the widely accepted conversion of 1 nm of thickness corresponds to ~1 ng/mm^2 surface density held reasonably well for these substances and through our experiments can now be further specified for different types of biomolecules. Through accurate calibration of the dependence of thickness on surface density, we have established a relation allowing precise determination of the absolute number of molecules for single-stranded DNA and two different proteins.

1. Introduction

Macromolecule interactions involving proteins and DNA are at the core of our understanding of cell biology and disease. The importance of techniques to interrogate these interactions via *in vitro* binding to a solid support, especially those that are high-throughput such as in arrayed systems, has been firmly established in both biological research and medicine (Stears et al., 2003; Predki, 2004; Macbeath and Schreiber, 2000; Zhu et al., 2001). Commonly, probe molecules are immobilized on a solid support using surface chemistry, target molecules are introduced in solution, and ensemble binding interactions between targets and probes are detected by fluorescently labeled secondary reagents (Espina et al., 2004). Although very successful for qualitative analyses, labeled fluorescence detection is an indirect measure of binding and molecular accumulation. Generating quantitative and real-time data with labeled techniques is difficult due to surface- and self-quenching at high densities (Ramdas et al., 2001), non-linear responses due to bleaching, lifetime and energy transfer issues (Song et al., 1995), and problems associated with quantifying responses between different fluorophores, assays, and measurement equipment. Additionally, the fluorescent molecules may alter the natural binding properties of the target molecules. As a result, complex calibrations are required for quantification of labeled signal response (Haab et al., 2001).

Label-free detection techniques have been developed for dynamic and quantitative sensing and have provided the advantages of simplicity and cost effectiveness (Ramachandran et al., 2005; Zhu and Snyder, 2003; Yu et al., 2006; Mitchell, 2002; Cooper, 2002). A leading technology in label-free sensing is the surface plasmon resonance (SPR) technique which has demonstrated quantitative and dynamic measurement capabilities (Jung et al., 1998; Campbell et al., 2002). Optical interferometric techniques that use layered substrates as solid supports for immobilized probes have gained attention as well because of their simplicity and sensitivity (Schmitt et al., 1997; Nikitin et al., 2005; Zhao et al., 2007; Bergstein et al., 2008; Özkumur et al., 2008). In interferometric approaches, the signal is created by an additional phase shift or optical path length difference (OPD) caused by the adsorbed biolayer.

* Corresponding author at: College of Engineering, 8 St. Mary's Street, Boston, MA 02215, USA. Tel.: +1 617 353 5067; fax: +1 617 353 6440.
E-mail address: selim@bu.edu (M.S. Ünlü).

0956-5663/$ – see front matter © 2009 Elsevier B.V. All rights reserved.
doi:10.1016/j.bios.2009.06.033

Table 1
Spotting volumes and concentrations of single-stranded DNA, BSA, and IgG.

ssDNA		BSA		IgG	
Concentration (μM)	Mean volume (pL)	Concentration (mg/mL)	Mean volume (pL)	Concentration (mg/mL)	Mean volume (pL)
0.9375	388	0.0625	388	0.0625	371
1.875	406	0.125	406	0.125	373
3.75	398	0.25	398	0.25	375
7.5	393	0.5	393	0.5	375
15	393	1	393	1	376
30 (0.22 mg/mL)	364	2	364	2	371

The concentration of DNA is given in units of μM and the others are shown in mg/mL. The concentration of the most concentrated DNA solution is shown in mg/mL as a reference. The molar mass of DNA was taken as 7245 g/mol as specified by the manufacturer.

The dielectric solid support materials are optically homogenous and have a uniform refractive index at the wavelengths used, implying a simple model where the optical path length that creates the phase delay is the product of the distance traveled and the refractive index. Here we validate this model for adsorbed layers of DNA and protein using an interferometric detection technique.

A similar investigation was conducted previously by De Feijter et al. They modeled adsorbed protein layers as having a fixed height based on the dimensions of the molecule with a variable refractive index based on surface concentration, and used ellipsometric measurements to validate their model (De Feijter et al., 1978). More recently, other investigators have made the approximation that adsorbed protein layers can be modeled as having a fixed index and a variable height (Schmitt et al., 1997; Nikitin et al., 2005). The aim of the present work is to validate the fixed-index model and to calibrate measured signals against known surface concentrations for DNA and protein.

We have recently introduced an interferometric technique termed Spectral Reflectance Imaging Biosensor (SRIB) that can detect label-free and dynamic biomolecular interactions in a high-throughput format (Özkumur et al., 2008). A silicon chip with a top layer of thick uniform oxide is used as the solid support for arrayed biomolecules. A tunable laser is incident on the array and reflection spectra are recorded for hundreds of spots simultaneously. The mass at each spot is found by measuring the phase difference between the biolayer and buried mirror reflections in the collected reflection spectra. A key advantage of SRIB over evanescent wave techniques such as SPR or waveguide sensors is that SRIB is highly insensitive to changes in temperature or buffer refractive index because the two reflections causing the phase shift are co-propagating. We have also recently shown that SRIB is insensitive to changes in molecular conformation on the surface, a topic that will be revisited in the discussion.

In our experiments, we detected the OPD for adsorbed protein and DNA using SRIB and calculated the height of the layers by assuming a uniform refractive index of $n = 1.45$. The height values were then compared to the known mass deposited on the surface. The ability to quantify mass by this method was assessed for oligomeric single-stranded DNA (ssDNA), bovine serum albumin (BSA), and immunoglobulin G (IgG) and results were compared with fluorescent measurements.

2. Materials and methods

2.1. Sample preparation and spotting of biomolecules

Silicon substrates with a thermal oxide of ~17 μm and 0.4 nm RMS roughness were purchased. Samples were cut to the size of standard microscope slides (25 mm × 75 mm) and cleaned. The surface treatment and spotting protocols used for the quantification and saturation coverage experiments are described below.

2.1.1. Calibration experiments

For the quantification experiments to demonstrate the linearity of SRIB measurements and calibrate the measured optical thickness with the adsorbed mass, no additional surface treatment was used. Spotting solutions were prepared by dissolving salt-free BSA, IgG, and ssDNA in milli-Q water so the resultant mass at each spot was entirely due to the macromolecules following the evaporation of water.

High purity salt-free (HPSF) single-strand DNA was purchased from Eurofins MWG Operon (Germany) and dissolved in milli-Q water to a concentration of 100 μM. Protein powders and spotted slides were kept in a sealed chamber containing a saturated solution of lithium bromide to control the environment humidity. All operations requiring the handling of dry protein powder or spotted slides were carried out in an inert argon atmosphere in a dry box.

Rabbit IgG and BSA (Sigma, St. Louis, MO) were dissolved in milli-Q water at a concentration of 10 mg/mL and extensively dialyzed using 12 kDa cut-off dialysis tubing (Sigma) against milli-Q water. After dialysis, the protein solutions were lyophilized and the resulting protein powders were re-dissolved by adding milli-Q water up to a final concentration of 2 mg/mL. Protein and DNA were serially diluted with milli-Q water using high precision pipettes from Gilson (Middleton, WI) down to the final concentrations reported in Table 1. The solutions were spotted using a Scienion SciFlexarrayer S5 (Berlin, Germany) piezoelectric arrayer equipped with the sciDropVOLUME software, a tool to measure the absolute volume of the droplets dispensed by a SciFlexarrayer piezo nozzle. For each spot, a photograph of the actual droplet in mid air is used to calculate the spotted volume. As an additional validation of the spot volumes, we spotted 10,000 times under identical experimental conditions and observed that the solution consumed was consistent with the average spot volume multiplied by 10,000 (data not shown).

For each biomolecule, 6 different concentrations were spotted in 2 rows of 10 spots each, forming 20 replicate spots for each concentration. Two identical slides, each spotted with two array replicates of 12 by 10, were prepared, yielding four replicate arrays for array-to-array and sample-to-sample comparison of the results. The average spotting volumes for three different biomolecules are given in Table 1.

For DNA, the total mass of a 23 *mer* of sequence 5′-NH_2-$(CH_2)_6$-GCC CAC CTA TAA GGT AAA AGT GA-3′ was calculated assuming a molar mass of 7.245 kDa. The predicted mass spotted was calculated by using the values given in Table 1. An oligonucleotide fragment of sequence: 5′-TCA CTT TTA CCT TAT AGG TGG GC-3′, labeled with Cy5, from Eurofins MWG Operon (Germany) was also spotted and scanned with a ProScanArray Microarray Scanner (PerkinElmer, MA, USA) for direct comparison of SRIB and fluorescence detection techniques.

2.1.2. Saturation coverage experiments

For the determination of saturation coverage, the surfaces were functionalized with a polymeric coating following procedures

Please cite this article in press as: Özkumur, E., et al., Biosens. Bioelectron. (2009), doi:10.1016/j.bios.2009.06.033

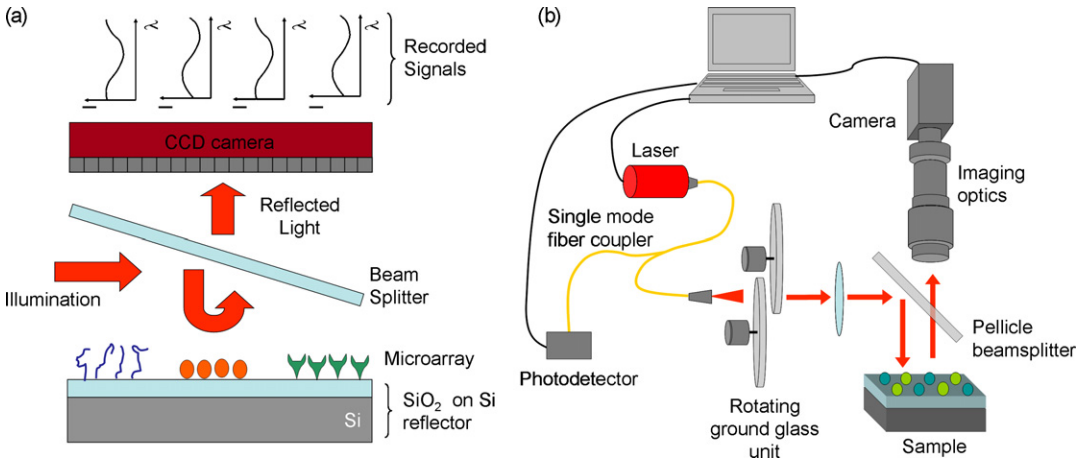

Fig. 1. (a) Basic working principle of the SRIB system. A tunable laser illuminates the surface and reflections from the surface are recorded by a CCD camera. Multiple reflections from the layered substrate form an interference pattern. This interference pattern is detectable on a CCD camera as intensity variations when the illumination wavelength is changed. Accumulation of biological material on the surface shifts the interference pattern which is detected by the corresponding pixels as a change in height. (b) Schematic of the SRIB system. The laser light is passed through a pair of rotating ground glass disks prior to illumination. Reflection is captured by a CCD camera using an imaging system that has variable zoom for optimizing the field of view to a variety of array sizes. The photodetector is used to track changes in the intensity of the laser.

described elsewhere (Cretich et al., 2004). The functional groups of the polymeric coating permit immobilization of biomolecules on the surface through covalent attachment to amine groups. Spotting solutions were prepared by dissolving BSA and IgG in phosphate buffered saline (PBS), and amine labeled ssDNA in 150 mM potassium phosphate buffer of pH 8.5. The same molecular concentrations given above for the quantification experiments were used. After spotting, the slides were kept in a 75% humidity chamber overnight at room temperature, and washed with PBS containing 0.1% Tween20, PBS only, and milli-Q water, then dried with argon before data acquisition using SRIB.

2.2. Optical setup and data acquisition

The SRIB technique has been described previously for label-free microarray sensing and imaging (Özkumur et al., 2008). A layered substrate consisting of thermally grown SiO_2 on Si is used as a solid support for biomolecules. The spectrum of light that is reflected from the substrate is modulated due to the reflections occurring at different interfaces and the frequency of this modulation determines the total OPD between the top surface and the buried surface reflections (SiO_2–Si interface). The interference between these reflections is an accurate measure of the optical phase delay which yields the thickness of this layer, including any adsorbed biomolecules. In the present work, the measured thickness is the combined result of the optical path length of the oxide alone plus the optical path length of the additional adsorbed material. The emission from a tunable laser (TLB6300, NewFocus, San Jose, CA) is passed through a rotating ground glass module to reduce the coherence-related speckle artifacts, then beam-expanded and incident on the sample. The reflected light is recorded by a CCD camera (Rolera-XR, QImaging, Surrey, BC, Canada) as a function of the laser wavelength for the entire field of view (FOV). Following data acquisition, the reflection spectrum at each pixel position is fit to an interference model to find the optical path difference between the reflections from the SiO_2 surface and the SiO_2–Si interface (Fig. 1a). High-throughput is provided by simultaneous recording of the phase information for the entire FOV.

The SRIB schematics is shown in Fig. 1b. The laser output is coupled to a 2×2 fiber coupler, with one arm attached to the apparatus illuminating the sample while the other arm is attached to a photodetector (PDA36A, Thorlabs, Newton, NJ) used to track intensity fluctuations of the laser. During data acquisition, the laser wavelength was scanned from 769 to 781 nm in 1 nm steps and 50 images were averaged at every wavelength to improve the data. The laser, photodetector, and camera were controlled with Labview software (National Instruments, Austin, TX).

2.3. Data processing

Following data acquisition, the interference curves at each pixel are fit to an interference model described previously, using a least squares approach (Özkumur et al., 2008). The OPD then results in a thickness value for each pixel using $n = 1.45$ which has been used elsewhere in the literature (Nikitin et al., 2005; Schmitt et al., 1997). The height of a spot was found by subtracting a reference thickness

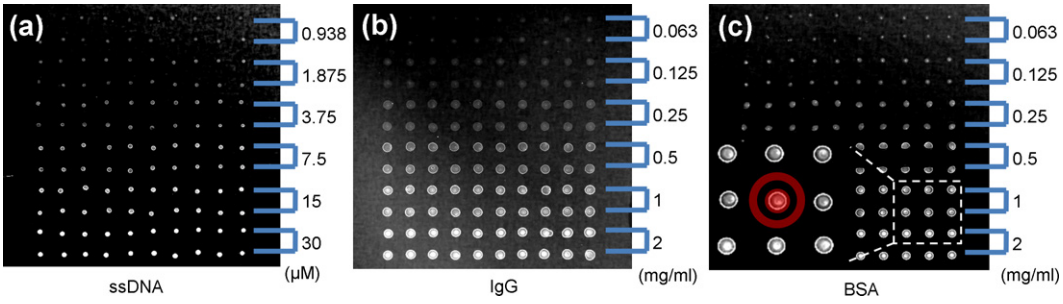

Fig. 2. Sample SRIB images of the arrays. 1 of 4 arrays spotted for each molecule is shown here. Each array contains 20 replicate spots for 6 different concentrations. The spot-to-spot distance is ~500 μm on all images. The height of a spot is calculated as shown in (c); by comparing the average of an inner circle with the average of an outer annulus.

Please cite this article in press as: Özkumur, E., et al., Biosens. Bioelectron. (2009), doi:10.1016/j.bios.2009.06.033

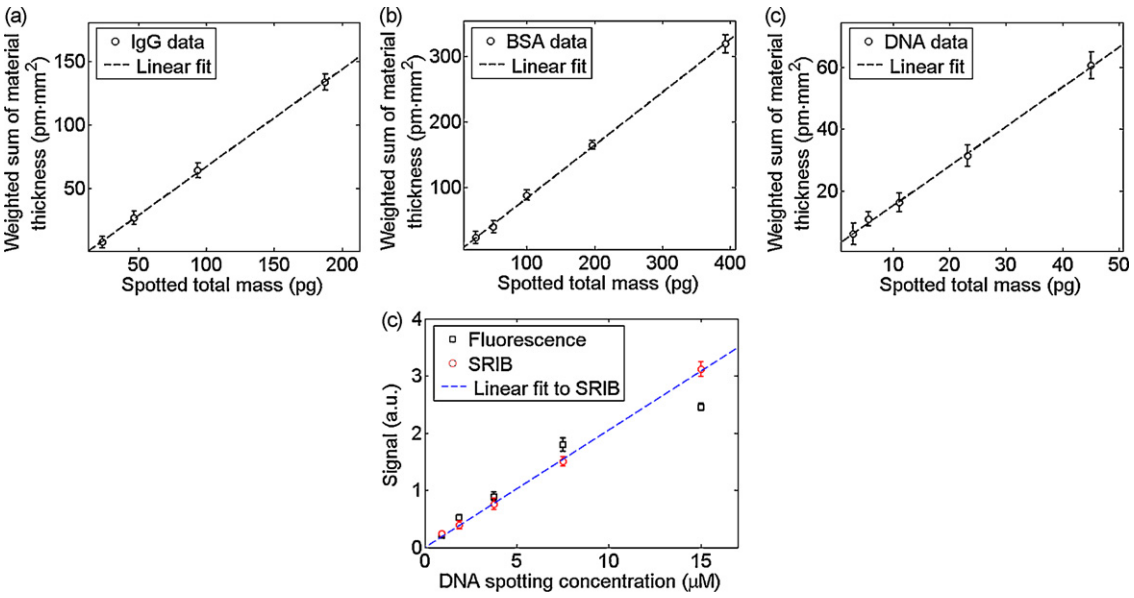

Fig. 3. SRIB measured results compared with the spotted mass. The data was acquired from each array by finding the average height of spots which is a measure of mass density. For valid comparison to total mass, the average height was multiplied by the area of the inner circle that was used to measure the height. This value is compared with the spotted mass of (a) IgG, (b) ssDNA, and (c) BSA. The error bars are the standard deviations of the spot-to-spot variation in the same array. (d) Comparison of SRIB response with fluorescence measurements. The spotted DNA array was scanned with a fluorescence scanner and the SRIB system before washing. The signals were normalized to plot them on the same graph. Note that in the case of DNA, even the highly concentrated spots are in the linear response regime of SRIB measurements. In all plots, the error-bars represent the standard deviation of measurements from spot-to-spot. Errors on the surface area estimation during the analysis are coupled into spot-to-spot variations and represented in the vertical-axis error-bars. A source of error for the horizontal axis is the variation of spotting volumes and it was measured to be insignificantly small. Therefore, no error-bars were used for the horizontal axis.

(oxide only) from the average total thickness arising from both the oxide and the bound molecules. The reference thickness was found by averaging the values of all pixels included in a ring surrounding the spot. The inner value was found by averaging all the pixels included in a circle that contains the entire spot (Fig. 2c). For IgG, with a maximum spot radius of ~70 μm, this would correspond to about 150 pixels averaged to determine the inner value.

3. Results

3.1. Linearity of SRIB measurements

The precise mass of ssDNA, BSA and IgG delivered to each spot on the surface was determined by carefully controlling the concentration of these macromolecules in salt-free water, accurately measuring the volume of liquid dispensed to each spot, and allowing the spots to dry completely. For each of the three different molecules, 4 arrays containing 120 spots were created. Each array was spotted with 6 different concentrations ranging over a factor of ~32, with 20 spots across two rows at each concentration. Fig. 2 shows an SRIB image of an array for each molecule. The height value for each spot was determined as described in Section 2 using a fixed-index model and this was compared with the spotted mass (via Table 1). The results of the SRIB measurements are shown in Fig. 3. In these plots, only the first 5 concentrations of ssDNA and BSA, and the first 4 concentrations of IgG are shown since the higher concentrations were beyond the linear response of SRIB. For the IgG spots with ~180 pg total mass, the spot radius was measured as ~70 μm, corresponding to a surface concentration close to 12 ng/mm^2. In this range of typical experimental layer densities of 20 ng/mm^2 and below, SRIB responses are linear. We measured the system noise floor at 5 pm when taking the measurements in dry environment (corresponding roughly to ~5 pg/mm^2, see Section 4), indicating the system has a dynamic range of ~4 orders of magnitude. According to our simulations, we expect a non-linear response as the layer thicknesses approach 20–30 nm, corresponding to 20–30 ng/mm^2. This is due in part to the layer thickness becoming a significant fraction of the wavelength and thus requiring a more detailed model, increasing layer non-uniformity for thick layers, and disparities between the empirical index and the assumed model index of 1.45. We observe this non-linear behavior for highly concentrated spots with surface densities greater than 20 ng/mm^2.

The SRIB linear dynamic range was also compared with fluorescence measurements by spotting fluorescently labeled DNA. The responses of both SRIB and the fluorescent scanner are plotted in Fig. 3d. Even though the amount of DNA in the highly concentrated spots is well above what is typically used, it nonetheless shows the superior linearity and dynamic range of SRIB measurements.

3.2. Relation between optical thickness and adsorbed mass

The linear relationship between spotted mass and the measured spot height was determined from the slopes of the fits to the data in Fig. 3. The surface concentration (pg/mm^2) is simply the known spotted mass divided by the measured spot area. Table 2 summarizes the resulting relationship between surface density and spot height; 1 nm of measured height correlates to surface concentrations of 1.21 ng/mm^2 for BSA, 1.28 ng/mm^2 for IgG, and 0.80 ng/mm^2 for DNA. In these measurements, the array-to-array variations of measured slope are on the order of 3%, a rather encour-

Table 2
Relationship between effective spot height (using a fixed refractive index of $n = 1.45$) and surface concentration for different macromolecules.

(ng/mm^2)/1 nm	Slide 1		Slide 2		Average
	Array 1	Array 2	Array 1	Array 2	
BSA	1.23	1.22	1.20	1.20	1.21
IgG	1.23	1.27	1.30	1.30	1.28
DNA	0.83	0.77	0.77	0.83	0.80

The measured slopes of the linear fits shown in Fig. 3 were compared to the measured spot areas to calculate the given values.

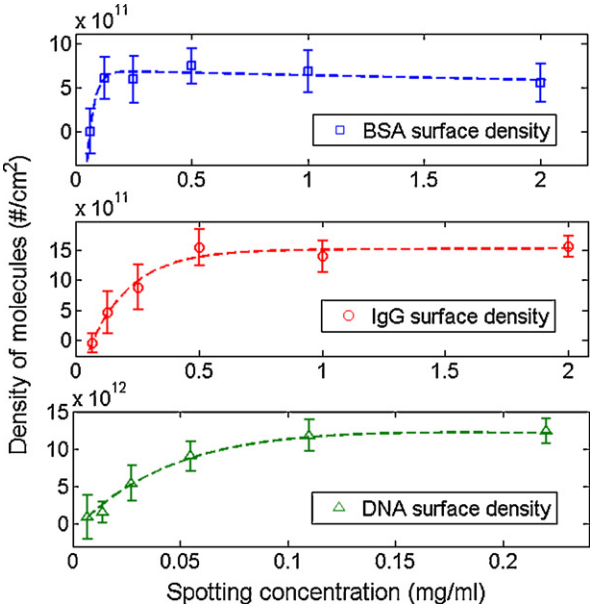

Fig. 4. Saturating surface concentration of BSA, IgG and ssDNA. The thickness-to-surface density conversion factors were used to find the surface concentration of adsorbed biomolecules. Increasing concentrations of the samples were spotted on a functionalized slide and the slide was washed to remove the unbound material after an overnight incubation. For BSA, the spot diameter increased with increasing spotting concentration causing an expanded spot morphology, and prevented the saturation of surface coverage. However, we measured saturation surface concentrations of 15×10^{11} molecules/cm^2 for IgG and 1×10^{13} molecules/cm^2 for ssDNA which agreed well with the theoretical and previously measured values.

aging empirical result. Note also that while these values are close to the generally accepted conversion between height and density, they differ by ~20% depending on the molecule.

3.3. Saturation surface coverage for IgG and BSA

To explore the saturation surface coverage of IgG, BSA and ssDNA, these molecules were spotted on the functionalized slides. The spotting and surface functionalization protocols are described in Section 2. The slides were imaged using SRIB after washing the excess unbound molecules. The optical thickness was determined for each spot and converted to mass density using the height-to-density conversions summarized in Table 2. The density of molecules was determined by dividing the measured mass density by the molecular weight of 66 kDa for BSA, 150 kDA for IgG and 7.245 kDa for ssDNA. Surface densities of biomolecules depending on the spotting concentrations are plotted in Fig. 4. For the BSA sample, the spot diameter increased rapidly as the spotting concentration increased, so the surface concentration saturated at $\sim 6 \times 10^{11}$ molecules/cm^2, well below the expected limit of surface coverage. For the IgG sample, however, surface coverage saturated at $\sim 15 \times 10^{11}$ molecules/cm^2, very close to the theoretical limit of 17×10^{11} molecules/cm^2 reported elsewhere (Oliviero et al., 2008). The saturation surface coverage for ssDNA was measured as $\sim 1 \times 10^{13}$ molecules/cm^2, which is consistent with the earlier studies that were conducted to characterize the polymeric surface coating (Pirri et al., 2004).

4. Discussion

Interferometric techniques for detecting label-free binding interactions on a surface generally assume a linear relationship between the OPD and bound macromolecule mass. Quantitative measurements require an experimentally verified model relating the phase delay to number of molecules (or mass) on the surface. Some investigations have modeled the OPD as the result of an adlayer of fixed-height with a refractive index that varies linearly from the bulk solution index to a saturating index for a monolayer, a model we refer to as the fixed-height approach (De Feijter et al., 1978; Voros, 2004; Davis and Wilson, 2000). Alternatively, others have assumed a fixed refractive index for the adsorbed layer, typically $n = 1.45$, and relate the OPD to an effective thickness or height, a model we refer to as fixed-index (Nikitin et al., 2005; Özkumur et al., 2008; Piehler et al., 1996; Moiseev et al., 2006). Ultimately, both the fixed-index and fixed-height approaches are approximations and a calibration with known concentrations of biomolecules on the surface is required. In this work, we have accomplished such a calibration for the SRIB system using the fixed-index model.

In the fixed-height model, refractive index and surface concentration are related to each other with the equation:

$$n_1 = n_2 + c_a \frac{dn}{dc} \quad (1)$$

where n_1 and n_2 are the refractive indices of the biolayer and surrounding medium (air or buffer), respectively, c_a is the surface concentration, and dn/dc is the incremental refractive index. This equation was validated by De Feijter et al. (1978) and they have found the incremental refractive index of a few proteins to be ~0.18 cm^3/g. Consistent results were shown in the literature using SPR (Davis and Wilson, 2000; Wolf et al., 2004). More importantly, the values reported for the incremental refractive index are consistent with those measured in bulk (Ball and Ramsden, 1998). This gives us confidence that adsorbed protein layers can be treated similarly even though tests have not been performed for each type of protein. This result is somewhat intuitive if one considers that the refractive index of the adsorbed layer is a function of the types of molecular bonds interacting with the light. The types of bonds in proteins arising from a distribution of the same amino acids are similar and their prevalence will scale with the number of bonds roughly as the mass of adsorbed protein, leading to this incremental refractive index.

Other approaches have taken the alternative model that the index of protein layers is fixed at $n = 1.45$ and it is the height that is varying linearly between 0 and a saturating level. The refractive index of adsorbed single-stranded DNA layers was also measured as $n = 1.46$ (Elhadj et al., 2004), conveniently close to protein layer approximation of $n = 1.45$. Gauglitz and co-workers have used the approximation of 1 pm height corresponding to 1 pg/mm^2 of biotin accumulation (Piehler et al., 1996) and Shumaker-Parry and Campbell showed a theoretical derivation for SPR signal approximating 1 pm to 1.3 pg/mm^2 of BSA or streptavidin (SA) (Campbell et al., 2002).

We have shown previously that for SRIB, the discrepancy between the fixed-height and fixed-index models is typically less than 5% for layer thicknesses smaller than the wavelength of light (Özkumur et al., 2008). Supporting this, we have recently shown that the conformational change of a polymeric coating on the surface did not significantly change the mass measurements (Yalçın et al., 2009). In an independent experiment, we determined that the polymer swelled from 2 to 20 nm when hydrated, allowing us to vary the refractive index of the layer significantly. Yet, this index change caused only about a 10% change in the detected thickness for SRIB measurements supporting our claim that the accuracy of measured thicknesses is independent of index and demonstrating that the accuracy of the SRIB system is insensitive to the model used.

Please cite this article in press as: Özkumur, E., et al., Biosens. Bioelectron. (2009), doi:10.1016/j.bios.2009.06.033

5. Conclusions

We have quantitatively calibrated the optical path difference in interferometric sensing to the surface-bound concentrations and masses of adsorbed layers of ssDNA, BSA, and IgG. Furthermore, we have shown that the correlation between OPD and bound mass can be well modeled with a fixed-index model with refractive index of $n = 1.45$, allowing us to calibrate the measured height to the absolute density of surface-bound molecules. We have demonstrated that our SRIB system has a linear dynamic range of nearly 4 orders of magnitude, which is comparable to standard SPR (Jung et al., 1998) and considerably better than imaging SPR (Campbell et al., 2002). We have also shown that label-free measurement of surface-bound DNA mass is comparable to fluorescence measurement methods for lower densities while being more linear across a wider range of surface concentrations. Finally, these results can be used to quantify protein-binding data, which has been difficult and challenging with fluorescence or other labeling techniques (Ramachandran et al., 2005; Bally et al., 2006).

References

Ball, V., Ramsden, J.J., 1998. Biopolymers 46, 489–492.
Bally, M., Halter, M., Voros, J., Grandin, H.M., 2006. Surface and Interface Analysis 38, 1442–1458.
Bergstein, D.A., Özkumur, E., Wu, A.C., Yalçın, A., Colson, J.R., Needham, J.W., Irani, R.J., Gershoni, J.M., Goldberg, B.B., Delisi, C., Ruane, M.F., Unlu, M.S., 2008. IEEE Journal of Selected Topics in Quantum Electronics 14, 131–139.
Campbell, C.T., Jung, L.S., Shumaker-Parry, J., 2002. Abstracts of Papers of the American Chemical Society 224, 255-ANYL.
Cooper, M.A., 2002. Nature Reviews Drug Discovery 1, 515–528.
Cretich, M., Pirri, G., Damin, F., Solinas, I., Chiari, M., 2004. Analytical Biochemistry 332, 67–74.
Davis, T.M., Wilson, W.D., 2000. Analytical Biochemistry 284, 348–353.
De Feijter, J.A., Benjamins, J., Veer, F.A., 1978. Biopolymers 17, 1759–1772.
Elhadj, S., Singh, G., Saraf, R.F., 2004. Langmuir 20, 5539–5543.
Espina, V., Woodhouse, E.C., Wulfkuhle, J., Asmussen, H.D., Petricoin, E.F., Liotta, L.A., 2004. Journal of Immunological Methods 290, 121–133.
Haab, B.B., Dunham, M.J., Brown, P.O., 2001. Genome Biology 2, RESEARCH0004.
Jung, L.S., Campbell, C.T., Chinowsky, T.M., Mar, M.N., Yee, S.S., 1998. Langmuir 14, 5636–5648.
Macbeath, G., Schreiber, S.L., 2000. Science 289, 1760–1763.
Mitchell, P., 2002. Nature Biotechnology 20, 225–229.
Moiseev, L., Unlu, M.S., Swan, A.K., Goldberg, B.B., Cantor, C.R., 2006. Proceedings of the National Academy of Sciences of the United States of America 103, 2623–2628.
Nikitin, P.I., Gorshkov, B.G., Nikitin, E.P., Ksenevich, T.I., 2005. Sensors and Actuators B-Chemical 111, 500–504.
Oliviero, G., Bergese, P., Canavese, G., Chiari, M., Colombi, P., Cretich, M., Damin, F., Fiorilli, S., Marasso, S.L., Ricciardi, C., Rivolo, P., Depero, L.E., 2008. Analytica Chimica Acta 630, 161–167.
Özkumur, E., Needham, J.W., Bergstein, D.A., Gonzalez, R., Cabodi, M., Gershoni, J.M., Goldberg, B.B., Unlu, M.S., 2008. Proceedings of the National Academy of Sciences of the United States of America 105, 7988–7992.
Piehler, J., Brecht, A., Gauglitz, G., 1996. Analytical Chemistry 68, 139–143.
Pirri, G., Damin, F., Chiari, M., Bontempi, E., Depero, L.E., 2004. Analytical Chemistry 76, 1352–1358.
Predki, P.F., 2004. Current Opinion in Chemical Biology 8, 8–13.
Ramachandran, N., Larson, D.N., Stark, P.R.H., Hainsworth, E., Labaer, J., 2005. FEBS Journal 272, 5412–5425.
Ramdas, L., Coombes, K.R., Baggerly, K., Abruzzo, L., Highsmith, W.E., Krogmann, T., Hamilton, S.R., Zhang, W., 2001. Genome Biology 2, RESEARCH0047.
Schmitt, H.M., Brecht, A., Piehler, J., Gauglitz, G., 1997. Biosensors and Bioelectronics 12, 809–816.
Song, L.L., Hennink, E.J., Young, I.T., Tanke, H.J., 1995. Biophysical Journal 68, 2588–2600.
Stears, R.L., Martinsky, T., Schena, M., 2003. Nature Medicine 9, 140–145.
Voros, J., 2004. Biophysical Journal 87, 553–561.
Wolf, L.K., Gao, Y., Georgiadis, R.M., 2004. Langmuir 20, 3357–3361.
Yalçın, A., Damin, F., Özkumur, E., Di Carlo, G., Goldberg, B.B., Chiari, M., Unlu, M.S., 2009. Analytical Chemistry 81, 625–630.
Yu, X.B., Xu, D.K., Cheng, Q., 2006. Proteomics 6, 5493–5503.
Zhao, M., Wang, X.F., Lawrence, G.M., Espinoza, P., Nolte, D.D., 2007. IEEE Journal of Selected Topics in Quantum Electronics 13, 1680–1690.
Zhu, H., Bilgin, M., Bangham, R., Hall, D., Casamayor, A., Bertone, P., Lan, N., Jansen, R., Bidlingmaier, S., Houfek, T., Mitchell, T., Miller, P., Dean, R.A., Gerstein, M., Snyder, M., 2001. Global analysis of protein activities using proteome chips. Science 293, 2101–2105.
Zhu, H., Snyder, M., 2003. Current Opinion in Chemical Biology 7, 55–63.

Please cite this article in press as: Özkumur, E., et al., Biosens. Bioelectron. (2009), doi:10.1016/j.bios.2009.06.033